SAN2015-10192J

Investigation of grain-scale microstructural variability in tantalum using crystal plasticity-finite element simulations

Hojun Lim[a,*], Rémi Dingreville[b], Lisa A. Deibler[c], Thomas E. Buchheit[a], Corbett C. Battaile[a]

[a] *Computational Materials and Data Science, Sandia National Laboratories, Albuquerque NM, 87185*
[b] *Structural and Thermal Analysis, Sandia National Laboratories, Albuquerque NM, 87185*
[c] *Materials Characterization and Performance, Sandia National Laboratories, Albuquerque NM, 87185*

Abstract

In this work, a crystal plasticity-finite element (CP-FE) model is used to investigate the effects of microstructural variability at a crack tip in tantalum single crystals and polycrystals. It is shown that at the macroscopic scale, the mechanical response of single crystals is sensitive to the crystallographic orientation while the response of polycrystals shows relatively small susceptibility to it. However, at the microscopic scale, the local stress and strain fields in the vicinity of the crack tip are completely determined by the local crystallographic orientation at the crack tip for both single and polycrystalline specimens with similar mechanical field distributions. Variability in the local metrics used (maximum von Mises stress and equivalent plastic strain at 3 % deformation) for 100 different realizations of polycrystals fluctuates by up to a factor of 2–7 depending on the local crystallographic texture. Comparison with experimental data shows that the CP model captures variability in stress-strain response of polycrystals that can be attributed to the grain-scale microstructural variability. This work provides a convenient approach to investigate fluctuations in the mechanical behavior of polycrystalline materials induced by grain morphology and crystallographic orientations.

Keywords: Crystal plasticity, Microstructure, Finite elements, Variability, Tantalum

1. Introduction

Most engineering-scale materials exhibit some inherent variability in their mechanical response, mainly due to an heterogeneous microstructure composed of disparate crystallographic texture, grain shapes and sizes, initial defect density, chemical compositions and phases. These microstructural variations affect both the local and global materials mechanical response. Quantitative study

*Corresponding author
Email address: hnlim@sandia.gov (Hojun Lim)

of material's variability is challenging since the number of materials features is large and available experimental and computational modeling tools generally provide incomplete and uncertain information on the phenomena of interest. Additionally, from a computational point of view, most conventional continuum-scale models are deterministic in nature, e.g. averaged, homogeneous material property of a polycrystal is assigned to represent the macroscopic behavior. Thus, localized stress and strain values arising from the microstructural features are ignored.

Crystal plasticity-finite element (CP-FE) models are becoming a powerful technique to predict microstructure-aware mechanical behaviors of polycrystalline materials in realistic time and length scales. Conventional crystal plasticity models use single crystal constitutive equations based on a dislocation slip on a pre-defined slip systems. In particular, CP-FE models have been directly applied to consider the effects of grain-scale microstructure to predict texture evolution and plastic anisotropy [1, 2, 3, 4, 5], inter- and intra-grain strain fields [6, 7, 8, 9, 10, 3, 11, 4, 5, 12], deformed specimen shapes [4, 5] and activated slips [13, 14, 6, 1]. Recently, CP-FE formulations have been used to investigate variability in materials's response, i.e. crack formation and growth [15] and fatigue [16]. In order to capture stochastic polycrystalline responses within a CP framework, stochastic plasticity deformation modes have been formulated [17, 18, 19] or microstructure is represented using probability density function (PDF) of grain morphology [20].

Alternatively, iterative simulations with many realizations of varying microstructure can be used to investigate material's variability [21, 22]. This approach eliminates assumptions on probabilistic distributions of materials behavior or plasticity processes. However, this method requires intensive computational expense to obtain reasonable statistics and becomes more taxing as the number of grains/elements are increased to represent realistic polycrystalline specimen dimensions.

In the present analysis, the iterative strategy mentioned above is used to investigate the effects of microstructural variability in a tantalum single crystals and polycrystals specimens. In particular, we focus on the effects of initial crystal orientations on materials' variability. One hundred realizations of single and polycrystalline notched specimens are generated and used in CP-FEM model to simulate plastic deformations upon uniaxial loading. Predicted grain scale variability from iterative simulations with varying microstructure is then used to compare with experimental measurements. This procedure allows more detailed investigation of stochastic mechanical responses in local stress and strain values as well as macroscopic behavior.

2. Crystal plasticity framework: Simulation procedures

In this work, a BCC crystal plasticity finite element model, developed at Sandia National Laboratories, was used to simulate deformation of single and polycrystalline tantalum specimens [23, 24]. The model is based on a well-established continuum formulation by Peirce et al. (PAN) [25] that follows multiplicative decomposition [26] of the deformation gradient $\mathbf{F}$ into a plastic component, $\mathbf{F}^{\mathrm{p}}$, representative of the motion of dislocations on active slip systems leaving the crystal lattice unrotated, and an elastic component, $\mathbf{F}^{\mathrm{e}}$, depicting the rotation and elastic stretching of the lattice. For isothermal conditions,

$$\mathbf{F} = \mathbf{F}^{\mathrm{e}} \cdot \mathbf{F}^{\mathrm{p}} \ . \tag{1}$$

Assuming plastic deformation is caused by dislocation slip, the plastic part of the velocity gradient, $\mathbf{L}_{\mathrm{p}}$, can be written as [25]:

$$\mathbf{L}_{\mathrm{p}} = \sum_{\alpha} \dot{\gamma}^{\alpha} \mathbf{s}_0^{\alpha} \otimes \mathbf{n}_0^{\alpha} \ , \tag{2}$$

where $\mathbf{s}_0^{\alpha}$ and $\mathbf{n}_0^{\alpha}$ are the initial slip direction and the slip plane normal direction on the α-th slip system, respectively. The slip rate on the α-th slip system, $\dot{\gamma}^{\alpha}$, is represented as a power-law function of resolved shear stress, τ^{α} and slip resistance, g^{α} [27]:

$$\dot{\gamma}^{\alpha} = \dot{\gamma}_0^{\alpha} \left(\frac{\tau^{\alpha}}{g^{\alpha}} \right)^{1/m} \ . \tag{3}$$

Here, $\dot{\gamma}_0^{\alpha}$ is the reference shear rate and m is the rate sensitivity factor. In this work, 24 $\{110\}\langle 111\rangle$ slip systems were used. The slip resistance, g^{α}, is composed of thermal and athermal parts as follows [24]:

$$g^{\alpha} = \min\left(\tau_{EI}^{*}, \tau_{LT}^{*}\right) + \tau_{\mathrm{obs}} \ , \tag{4}$$

where, $\min\left(\tau_{EI}^{*}, \tau_{LT}^{*}\right)$ is the temperature and strain rate dependent lattice resistance based on dislocation kink-pair theory [28, 29, 30, 31, 24] while τ_{obs} is the resistance due to obstacles. τ_{EI}^{*} and τ_{LT}^{*} denote lattice resistances at different temperature/ stress regimes using the dislocation elastic interaction (EI) model and the dislocation line tension (LT) model, respectively. Note that EI and LT models correspond to thermal parts of the flow stress at high temperature/ low stress regime and low temperature/ high stress regime, respectively.

τ^*_{EI} and τ^*_{LT} can be represented as follows:

$$\tau^{*\alpha}_{EI} = \tau^{EI}_0 \left(1 - \frac{k_{\mathrm{B}} T \ln(\dot{\varepsilon}_0/\dot{\gamma}^\alpha)}{2H_k}\right)^2 , \tag{5}$$

$$\tau^{*\alpha}_{LT} = \tau^{LT}_0 \left(1 - \left[\frac{k_{\mathrm{B}} T \ln(\dot{\varepsilon}_0/\dot{\gamma}^\alpha)}{2H_k}\right]^{1/2}\right) , \tag{6}$$

where T is the temperature, H_k is the formation enthalpy of an isolated kink, k_{B} is Boltzmann's constant and $\dot{\varepsilon}_0$ is the reference shear rate and τ^{EI}_0 and τ^{LT}_0 are material parameters.

The resistance due to obstacles, τ_{obs}, in Equation (4) is assumed to be athermal and is governed by dislocation-dislocation or dislocation-obstacle interactions. In commercially pure tantalum with large grains, the main contribution to this resistance should be from dislocation-dislocation interactions. Thus, the obstacle strength hardens and is formulated using forest dislocation densities as follows [32, 33]:

$$\tau_{\mathrm{obs}} = A\mu \mathrm{b} \sqrt{\sum_{\beta=1}^{\mathrm{NS}} \rho^\beta} . \tag{7}$$

Here, A is a material constant usually in the range of 0.3–0.6 [34], μ is the shear modulus, b is the Burger's vector, NS is the total number of slip systems, and ρ^β is the dislocation density on slip system β. It is assumed that initial dislocation densities are identical for all 24 slip systems and the evolution of dislocation density for the α-th slip system is obtained by a standard phenomenological equation [35]:

$$\dot{\rho}^\alpha = \left(\kappa_1 \sqrt{\sum_{\beta=1}^{\mathrm{NS}} \rho^\beta} - \kappa_2 \rho^\alpha\right) \cdot |\dot{\gamma}^\alpha| , \tag{8}$$

where, κ_1 and κ_2 are material parameters representing generation and annihilation of dislocations, respectively. Parameters κ_1 and κ_2 determine the shape of the strain hardening curve and can be obtained by fitting the model to measured stress-strain data.

Material constants used in the simulations are listed in Table 1. Note that τ^{LT}_0, τ^{EI}_0, $\dot{\varepsilon}_0$ and $2H_k$ were obtained by fitting the EI and LT models to tantalum single crystal experiments [37, 24] while hardening parameters, κ_1 and κ_2, and the initial obstacle strength, $\tau_{\mathrm{obs},0}$ were parameterized from the measured stress-strain data [38]. Elastic constants and the Burger's vector for tantalum were obtained from the literature [36]. More detailed description of the model are discussed in a recent paper by [38].

Table 1: Material parameters used in the tantalum oligocrystal simulations [36, 24].

Parameters	Values	Parameters	Values	Parameters	Values	Parameters	Values
m	0.012	τ_0^{LT}	406 MPa	C_{11}	267 GPa	κ_1	1.4×10^6 m^{-1}
$\dot{\gamma}_0$	0.001 s^{-1}	τ_0^{EI}	320 MPa	C_{12}	161 GPa	κ_2	14
A	0.4	$2H_k$	0.85 eV	C_{44}	82.5 GPa	$\tau_{\text{obs},0}$	27 MPa
b	2.87 Å	$\dot{\varepsilon}_0$	2.99×10^6 s^{-1}	μ	70.7 GPa		

Using CP-FE model for tantalum, plastic deformations of notched specimens having different microstructures are simulated. Figure 1 shows the dimension of the notched tantalum specimen. The dimension of the specimen is 1000 μm $\times$ 1000μm $\times$ 2μm and the notch has a rounded tip with a radius of 8 μm. Figures 2 (a)–(d) show four different microstructures having 1, 204, 483 and

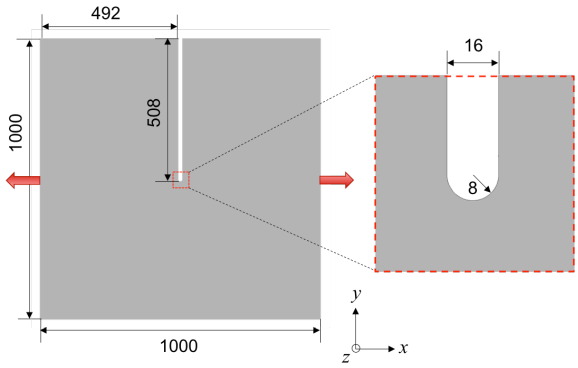

Figure 1: Dimension of the notched tantalum specimen. Uniaxial tension is applied along x-direction at a nominal strain rate of 10^{-4} s^{-1}.

1184 equiaxed grains. The three polycrystalline microstructures in Figs. 2 (b)–(d) were obtained from two-dimensional Monte Carlo Potts grain growth simulations. A splined mesh was created by fitting cubic splines to the vertices to mitigate artificial stress/ strain localizations that could occur from voxelated mesh. A single finite element was used through the thickness and total numbers of 111696, 115579, 111696 and 83657 eight-boded hexahedral finite elements were used to present four microstructures. The displacements along x-direction were applied on the nodes at the x surfaces of the mesh. The total displacement of 30 μm which correspond to 3% engineering strain was applied at the normal strain rate of $\dot{\varepsilon} = 10^{-4}$ s^{-1}. Plane strain boundary conditions in z-surfaces were applied. The total of 100 simulations were conducted for each case with varying crystal orientations. For each simulation, random initial crystal orientations are assigned. Note that the grain shapes,

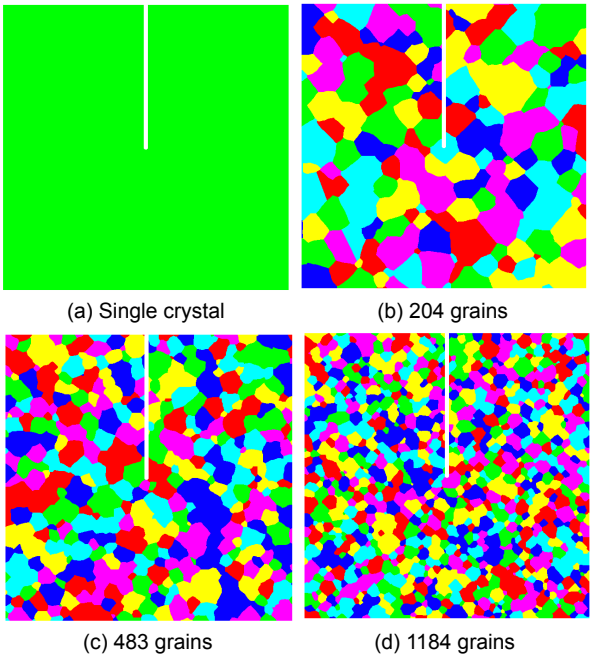

Figure 2: (a) Four microstructures of the notch specimen having (a) single grain, (b) 204 grains, (c) 483 grains and (d) 1184 grains.

material parameters, boundary conditions and geometries of the specimens were identical for each microstructure.

3. Macroscale vs. microscale variability at the crack tip

Figures 3 (a)–(d) show simulated the load-displacement curves from 100 realizations by varying the initial crystallographic orientations (random texture) for each microstructure. It is shown that the variability in the macroscopic flow curve is large in the case of single crystals, it decreases as the number of grains are increased. For a single crystal, the load at the displacement of 30 μm (3 % deformation) ranges from 0.198 to 0.402 N while it ranges from 0.253 to 0.292 N for 1184 grains. Thus the ratios between the maximum and minimum load from 100 simulations at a macroscopic deformation of 3 %, attributed solely to the initial grain orientation, is 2.03 for a single crystal while 1.21, 1.18 and 1.16 for specimens having 204, 483 and 1184 grains, respectively. Note that the single crystals represent extreme textures in polycrystals and thus variation from single crystal data can be used as upper and lower limits of the macroscopic behavior that arises from varying crystallograhic texture. On the other hand, average loads at 3 % deformation from 100 simulations are similar for single and polycrystals: 0.259 N for a single crystal case and 0.259–0.270 N for

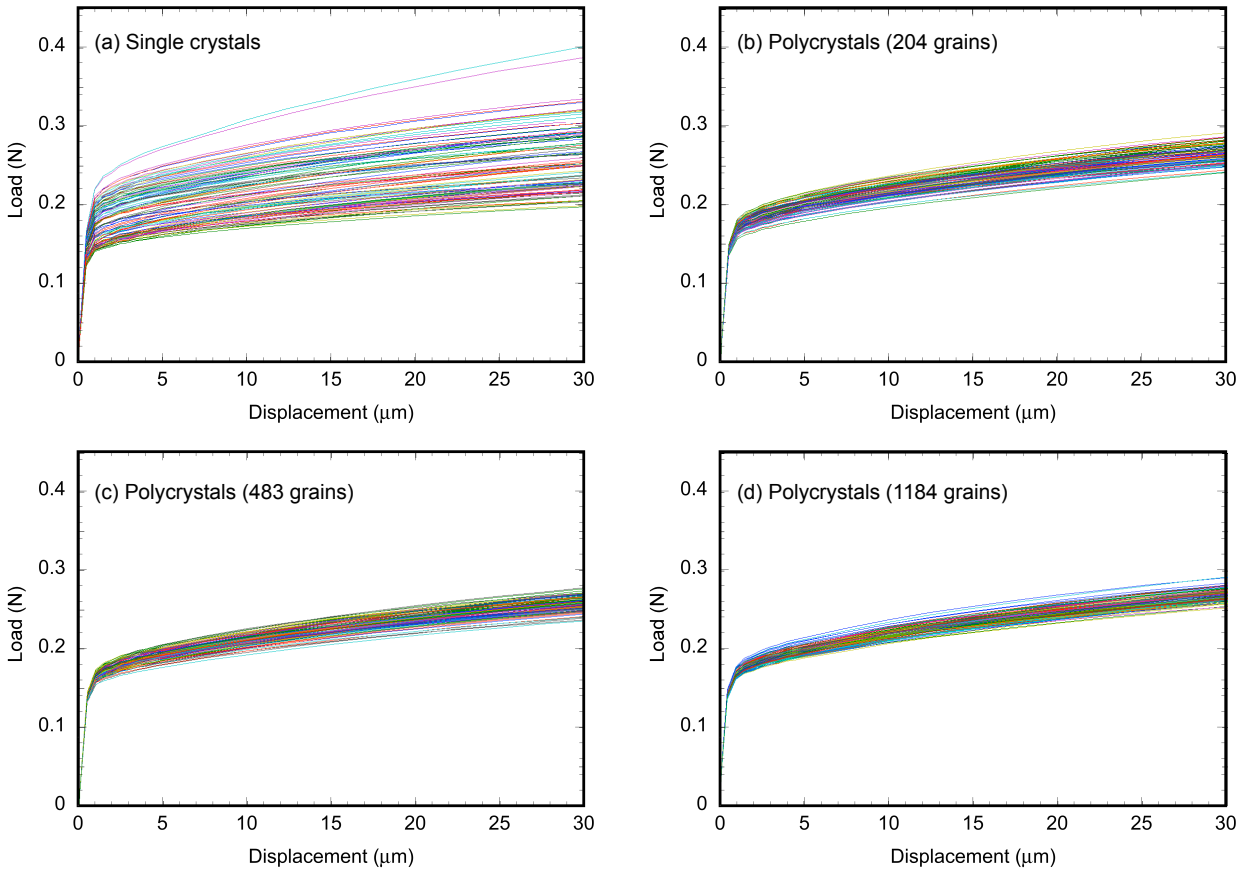

Figure 3: Load-displacement curves from 100 realizations by varying initial crystal orientations having (a) single grain, (b) 204 grains, (c) 483 grains and (d) 1184 grains. Specimens were deformed up to 3 %.

polycrystalline simulations. In order to quantify the localized stress and strain values, von Mises stress ($\sigma_{\rm VM}$) and equivalent plastic strain ($\bar{\varepsilon}_{\rm p}$) metrics are being used.

$$\sigma_{\rm VM} = \sqrt{\frac{3}{2}\sigma_{ij}\sigma_{ij} - \frac{1}{2}\left(\sigma_{kk}\right)^2}\ , \tag{9}$$

$$\bar{\varepsilon}_{\rm p} = \int_0^t \sqrt{\frac{2}{3}\mathbf{F}^{\rm p} : \mathbf{F}^{\rm p}}dt\ . \tag{10}$$

For each simulation, the maximum $\sigma_{\rm VM}$ and $\bar{\varepsilon}_{\rm p}$ values within the whole specimen,$\sigma_{\rm VM}^{\rm max}$ and $\bar{\varepsilon}_{\rm p}^{\rm max}$, are obtained. Obviously, these maxima are located in the vicinity of the crack tip regardless of the realization and correspond to stress concentration at the crack tip. Figures 4 (a)–(c) compare probabilities of load, maximum $\sigma_{\rm VM}^{\rm max}$ and maximum $\bar{\varepsilon}_{\rm p}^{\rm max}$ distributions for each microstructure at 3 % deformation. Here, probabilities of simulated values are plotted using a Gaussian distribution. It is shown that the single crystal has a wider distribution of load compared to polycrystals

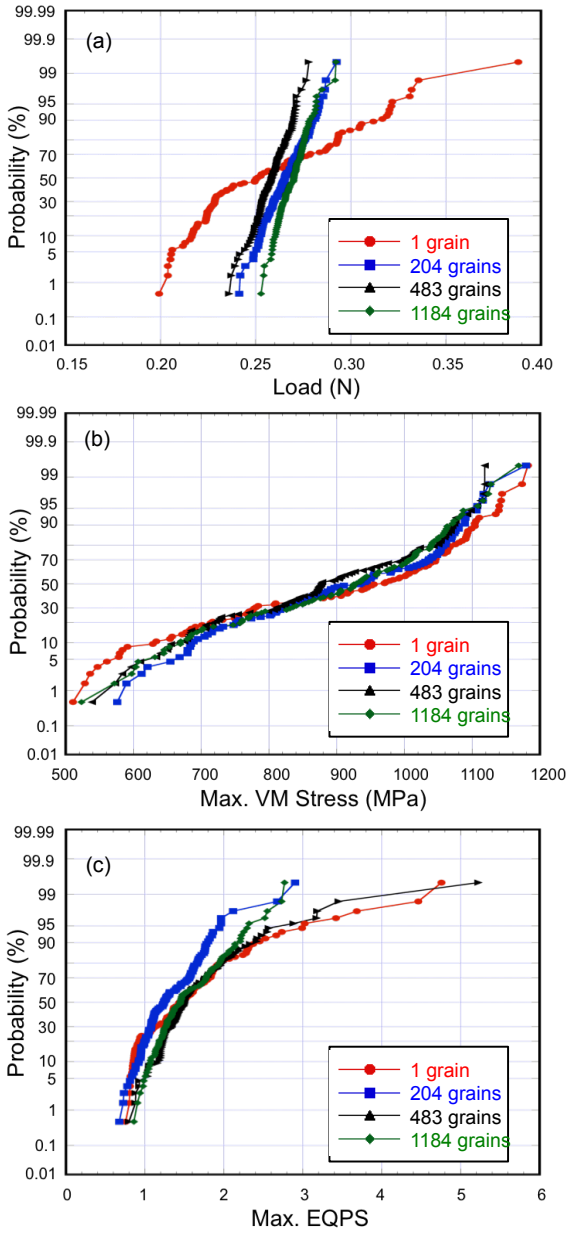

Figure 4: Probabilities of (a) load, (b) maximum von Mises stress ($\sigma_{\mathrm{VM}}^{\mathrm{max}}$), and (c) equivalent plastic strain ($\bar{\varepsilon}_{\mathrm{p}}^{\mathrm{max}}$) distributions at 3 % deformation from 100 realizations.

Table 2: Predicted load, maximum von Mises (VM) stress,$\sigma_{\mathrm{VM}}^{\mathrm{max}}$, and equivalent plastic strain (EQPS), $\bar{\varepsilon}_{\mathrm{p}}^{\mathrm{max}}$, within a whole specimen at 30 μm displacement from 100 realizations. Here, max./min. represents ratio between the largest and smallest values from 100 simulations.

	Load (N)			$\boldsymbol{\sigma_{\mathrm{VM}}^{\mathrm{max}}}$ **(MPa)**			$\boldsymbol{\bar{\varepsilon}_{\mathrm{p}}^{\mathrm{max}}}$		
Microstructure	max./min.	avg.	std. dev.	max./min.	avg.	std. dev.	max./min.	avg.	std. dev.
1 grain	2.03	0.259	0.040	2.30	792	185	6.83	1.60	0.73
204 grains	1.21	0.266	0.011	2.16	791	151	4.29	1.33	0.39
483 grains	1.18	0.259	0.009	2.00	820	153	6.55	1.66	0.62
1184 grains	1.16	0.270	0.008	2.21	801	152	3.21	1.55	0.43

(Fig. 4 (a)), while the maximum $\sigma_{\mathrm{VM}}^{\mathrm{max}}$ and maximum $\bar{\varepsilon}_{\mathrm{p}}^{\mathrm{max}}$ show similar distributions for single and polycrystalline specimens (Fig. 4 (b) and (c)). Table 2 summarizes predicted load, $\sigma_{\mathrm{VM}}^{\mathrm{max}}$ and $\bar{\varepsilon}_{\mathrm{p}}^{\mathrm{max}}$ values at 3 % deformation. The ratios between the largest and smallest (max/min) load from 100 simulations decreases as the number of grains increases. Additionally, no correlation is found between the number of grains and the max./min. values of $\sigma_{\mathrm{VM}}^{\mathrm{max}}$ and $\bar{\varepsilon}_{\mathrm{p}}^{\mathrm{max}}$. Interestingly enough, all four curves in Figs. 4 (b) and (c) show almost identical distributions.

Results displayed in Fig. 4 suggest that the variability in macroscopic response is relatively small for a polycrystals while the local properties show large variations depending on the local microstructure. It is shown that the maximum von Mises stress or equivalent plastic strain can be varied by up to a factor of 2–7 depending on the local crystal orientations. This implies that localized events such as failure and fracture that significantly depend on the local state of stress and strain will be affected by the grain scale microstructure. It should be noted that most damage metrics in a continuum damage mechanics (CDM) are composed of local stress or strain measures [39, 40]. Thus, it can be assumed that the damage metrics would have similar variations depending on the microstructure. This may explain relatively large variability in ductility (see experimental validation in Section 4) compared to yield stress or ultimate tensile stress in polycrystalline tensile tests. Figures 5 (a) and (b) illustrate the variation of the load versus the maximum von Mises stress values ($\sigma_{\mathrm{VM}}^{\mathrm{max}}$) for a single and polycrystals having 204 grains at 3% deformation. A linear correlation between the macroscopic load and the localized maximum von Mises stress for a single crystal case is observed whereas polycrystals do not show such correlation. Figure 5 suggests that the crystal orientation in a single crystal directly determines the macroscopic response as well as the local stress. However, in polycrystals, local microstructure at the tip determines the local stress but does not have significant influence on the global response. Figure 6 shows the variation of $\sigma_{\mathrm{VM}}^{\mathrm{max}}$

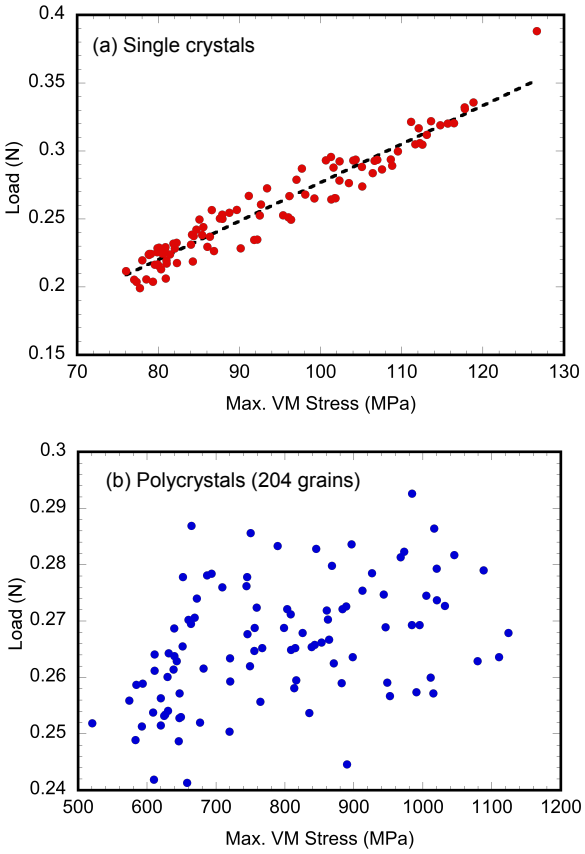

Figure 5: Plots of load versus the maximum von Mises stress ($\sigma_{\mathrm{VM}}^{\mathrm{max}}$) at 3% deformation for (a) single crystal and (b) polycrystal having 204 grains.

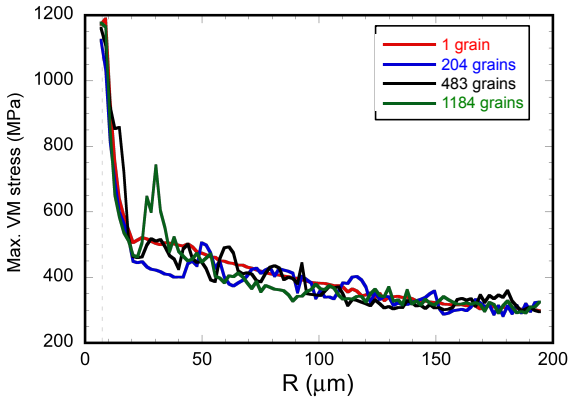

Figure 6: A plot of maximum von Mises stress versus the distance from the notch.

as a function of the distance away from the notch. Here, maximum values from 100 simulations are chosen. Similar to probability distribution, all four cases show similar local stress profile except for some peaks that arise from elastic incompatibilities arising from two adjacent grains.

4. Comparisons with experiments

In order to compare simulated materials' grain scale variability with observed experimental measurements, iterative tensile tests were conducted using polycrystalline tantalum specimens. Polycrystalline tantalum sheet, provided from HC Starck, was clock rolled and asymmetric tilt rolled to obtain uniform texture [41]. The average grain size is 32 μm. Three ASTM E08 sub-size samples and 45 samples scaled to 1/2 size of the ASTM E08 sub-size samples were machined from various locations of a single tantalum plate. Note that there was slight variation of the microstructure at different locations of the plate. The average grain sizes near the center of the plate were around 24–27 μm while the grains near the edge were 38–40 μm. Aspect ratios of the grains were larger near the center (aspect ratio=1.6) compared to edge of the plate where grains were close to equiaxed (aspect ratio=1.1). Figure 7 shows the SEM image of tantalum specimen obtained from the various locations of the plate. Forty-eight tensile tests were performed at a

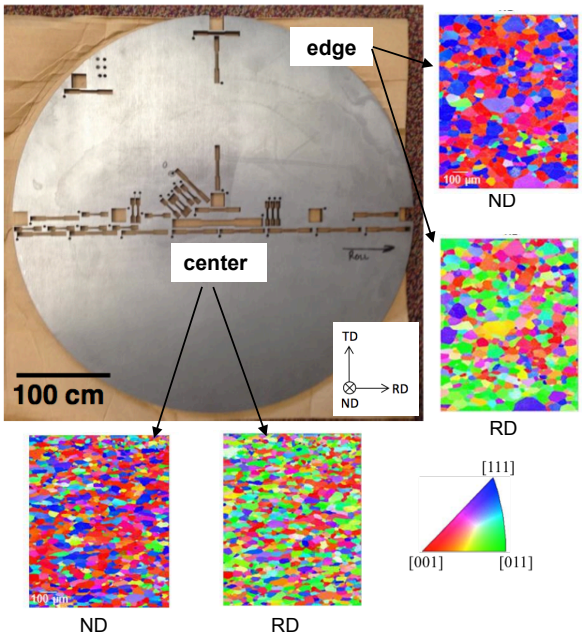

Figure 7: SEM images of the tantalum specimen in RD and ND from various locations of the plate.

nominal strain rate of $1.33 \times 10^{-3}\text{s}^{-1}$ at room temperature on a servo-hydraulic MTS load frame

equipped with a 5000 lb load cell. Strain measurements were performed using both a non-contact Epsilon Tech LE-01 laser extensometer and a MTS 100 % 0.5 in. clip extensometer to capture both high resolution strain data and strain measurement throughout the whole strain range.

Iterative CP-FE simulations of polycrystalline tantalum were conducted using a polycrystalline mesh having 201 grains, as shown in Figure 7 (b). A total of 60297 hexahedral finite elements were used. In order to accurately reproduce the experiment, the specimen was deformed up to 20 % at the strain rate of 1.33 $\times 10^{-3}$ s^{-1}. In addition, the hardening parameters were adjusted to reproduce averaged engineering stress-strain curves; $\tau_{obs,0} = 10MPa$, $\kappa_1 = 10^6$ m^{-1} and $\kappa_2 = 10$ were used. Similar to simulation procedures in the previous section, random crystal orientations were assigned to each grain and 100 realization of the the microstructure by varying initial crystal orientations were generated and simulated. Figures 8 (a) and (b) show measured and predicted

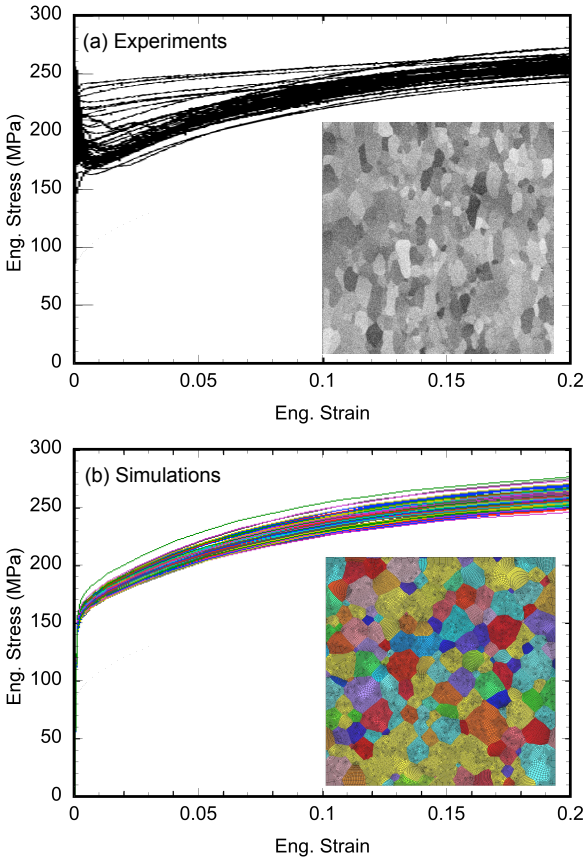

Figure 8: Stress-strain responses of polycrystalline tantalum obtained from (a) 48 tensile experiments and (b) 100 CP-FE simulations and corresponding microstructures.

stress-strain responses of the polycrystalline tantalum. The CP-FE model was unable to reproduce the upper and lower yield phenomenon observed in experiments. However, the variability of the

simulated stress-strain response at high strain regimes agree relatively well with measured data. Also note that the failure strains from the experiments had large variation, from 0.20–0.85, while the deviation in ultimate tensile strength (UTS) were within 10 % deviation. This can be correlated to and put in parallel with the results from the previous section that model predicts larger variation in local $\sigma_{\mathrm{VM}}^{\max}$ and $\bar{\varepsilon}_{\mathrm{p}}^{\max}$, and small deviation in global stress.

5. Discussion and Conclusions

Although the current approach is suitable to study the effects of grain scale microstructure variability on mechanical behaviors of single and polycrystalline metals, detailed physics or mechanisms can be incorporated into crystal plasticity model to understand the materials' stochastic behavior of interest. For example, dislocation-grain boundary interaction model is required to introduce the length scale, i.e. grain size effects. Furthermore, effects of other heterogeneous microstructural features such as grain shapes, initial defect density and chemical composition should be considered to fully quantify the uncertainties in materials response.

In this work, crystal plasticity finite element model was used to investigate the influence of initial crystal orientations on mechanical behaviors of polycrystalline tantalum. In particular, it is shown that the single crystal simulations may provide extreme cases for polycrystals in macroscopic mechanical behavior. Furthermore, localized stochastic behaviors were similar in single and polycrystals. Although the current work neglects some detailed microstructural features, this work provides an insight to stochastic analysis and uncertainty quantification that attribute to grain-scale microstructure using crystal plasticity simulations. Here are the main conclusions of the work.

- Single crystals showed large variation in macroscopic responses depending on the grain orientation. As the number of grains is increased, smaller variation is observed.
- Single crystal simulations provide upper and lower bounds of macroscopic yield behavior for polycrystals.
- Distribution of localized stress and strain are similar for both single and polycrystals.
- Localized stress and strain values are determined by the local crystal orientation. Thus, there is little correlation between the maximum stress/ strain values and macroscopic response.
- Predicted variations in flow stress agree well with experimental measurements.

Acknowledgement

The authors would like to thank Tyler Payton and Tom Crenshaw for mechanical testing support. Supported by the Laboratory Directed Research and Development program at Sandia National Laboratories, a multi-program laboratory managed and operated by Sandia Corporation, a wholly owned subsidiary of Lockheed Martin Corporation, for the U.S. Department of Energy's National Nuclear Security Administration under contract DE–AC04–94AL85000.

References

[1] F. Delaire, J. L. Raphanel, C. Rey, Plastic heterogeneities of a copper multicrystal deformed in uniaxial tension: Experimental study and finite element simulations, Acta Mater. 48 (2000) 1075–1087.

[2] K. Cheong, E. P. Busso, Effects of lattice misorientations on strain heterogeneities in fcc polycrystals, J. Mech. Phys. Sol. 54 (2006) 671–689.

[3] Z. Zhao, M. Ramesh, D. Raabe, A. Cuitiño, R. Radovitzky, Experimental investigation of plastic grain interaction, Int. J. Plast. 24 (2008) 2278–2297.

[4] B. Klusemann, B. Svendsen, H. Vehoff, Investigation of the deformation behavior of Fe-3%Si sheet metal with large grains via crystal plasticity and finite-element modeling, Comp. Mater. Sci. 52 (2012) 25–32.

[5] B. Klusemann, B. Svendsen, H. Vehoff, Modeling and simulation of deformation behavior, orientation gradient development and heterogeneous hardening in thin sheets with coarse texture, Int. J. Plast. 50 (2013) 109–126.

[6] A. Ziegenbein, H. Neuhäuser, J. Thesing, R. Ritter, H. Wittich, E. Steck, M. Levermann, E. Woldt, Local plasticity of Cu-AI polycrystals - measurements and FEM-simulation, J. Phys. IV France 8 (1998) 407–412.

[7] D. Raabe, Z. Z. M. Sachtleber, F. Roters, S. Zaefferer, Micromechanical and macromechanical effects in grain scale polycrystal plasticity experimentation and simulation, Acta Mater. 49 (2001) 3433–3441.

[8] M. Sachtleber, Z. Zhao, D. Raabe, Experimental investigation of plastic grain interaction, Mat. Sci. Eng. A 336 (2002) 81–87.

[9] T. Hoc, J. Crépin, L. Gélébart, A. Zaoui, A procedure for identifying the plastic behavior of single crystals from the local response of polycrystals, Acta Mater. 51 (2003) 5477–5488.

[10] E. Héripré, M. Dexet, J. Crépin, L. Gélébart, A. Roos, M. Bornert, D. Caldemaison, Coupling between experimental measurements and polycrystal finite element calculations for micromechanical study of metallic materials, Int. J. Plast. 23 (2007) 1512–1539.

[11] C. Badulescu, M. Grédiac, H. Haddadi, J.-D. Mathias, X. Balandraud, H.-S. Tran, Applying the grid method and infrared thermography to investigate plastic deformation in aluminium multicrystal, Mech. Mater. 43 (2011) 36–53.

[12] T. J. Turner, P. A. Shade, J. C. Schuren, M. Groeber, The influence of microstructure on surface strain distributions in a nickel micro-tension specimen, Modell. Sim. Mater. Sci. Eng. 21 (2013) 015002.

[13] F. Havlíček, J. Kratochvil, M. Tokuda, V. Lev, Finite element model of plastically deformed multicrystal, Int. J. Plast. 6 (1990) 281–291.

[14] Z. Yao, R. H. Wagoner, Active slip in aluminum multicrystals, Acta metall. mater. 41 (1993) 451–468.

[15] G. M. Owolabi, H. A. Whitworth, Modeling and simulation of microstructurally small crack formation and growth in notched nickel-base superalloy component, J. Mater. Sci. Technol. 30 (2014) 203–212.

[16] D. L. McDowell, Simulation-based strategies for microstructure-sensitive fatigue modeling, Materials Science and Engineering A 468-470 (2007) 4–14.

[17] L. Zhang, R. Dingreville, T. Bartel, M. T. Lusk, A stochastic approach to capture crystal plasticity, Int. J. Plast. 9 (2011) 1432–1444.

[18] P. Lin, Z. Liu, Y. Cui, Z. Zhuang, A stochastic crystal plasticity model with size-dependent and intermittent strain bursts characteristics at micron scale, International Journal of Solids and Structures 69-70 (2015) 267–276.

[19] H. Askari, M. R. Maughan, N. Abdolrahim, D. Sagapuram, D. F. Bahr, H. M. Zbib, A stochastic crystal plasticity framework for deformation of micro-scale polycrystalline materials, International Journal of Plasticity 68 (2015) 21–33.

[20] S. Sankaran, N. Zabaras, Computing property variability of polycrystals induced by grain size and orientation uncertainties, Act Mater. 55 (2007) 2279–2290.

[21] J. E. Bishop, J. M. Emery, R. V. Field, C. R. Weinberger, D. J. Littlewood, Direct numerical simulations in solid mechanics for understanding the macroscale effects of microscale material variability, Computer Methods in Applied Mechanics and Engineering 287 (2015) 262–289.

[22] K. Teferra, L. Graham-Brady, Tessellation growth models for polycrystalline microstructures, Computational Materials Science 102 (2015) 57–67.

[23] H. Lim, C. R. Weinberger, C. C. Battaile, T. E. Buchheit, Application of generalized non-Schmid yield law to low temperature plasticity in bcc transition metals, Model. Simul. Mater. Sci. Eng. 21 (2013) 045015.

[24] H. Lim, C. C. Battaile, J. D. Carroll, B. L. Boyce, C. R. Weinberger, A physically based temperature and strain rate dependent crystal plasticity model for bcc metals, J. Mech. Phys. Sol. 74 (2015) 80–96.

[25] D. Peirce, R. J. Asaro, A. Needleman, An analysis of nonuniform and localized deformation in ductile single crystals, Acta Metall. 30 (1982) 1087–1119.

[26] E. H. Lee, Elastic-plastic deformation at finite strains, Appl. Mech. 36 (1969) 1–6.

[27] J. W. Hutchinson, Bounds and self-consistent estimates for creep of polycrystalline materials, Proc. R. Soc. Lond. A 348 (1976) 101–127.

[28] A. Seeger, The temperature and strain-rate dependence of the flow stress of body-centered cubic metals: A theory based on kink–kink interactions, Z. Metallikd 72 (1981) 369–380.

[29] A. Seeger, Why anomalous slip in body-centred cubic metals?, Mater. Sci. Eng. A 319-321 (2001) 254–260.

[30] A. Argon, Strengthening mechanisms in crystal plasticity, Oxford University Press, 2008.

[31] M. Z. Butt, Kinetics of flow stress in crystals with high intrinsic lattice friction, Philos. Mag. 87 (2007) 3595–3614.

[32] G. I. Taylor, The mechanism of plastic deformation of crystals. Part I. Theoretical, Proc. Roy. Soc. A 165 (1934) 362–387.

[33] R. Dingreville, C. C. Battaile, L. N. Brewer, E. A. Holm, B. L. Boyce, The effect of microstructural representation on simulations of microplastic ratcheting, Int. J. Plast. 21 (2010) 617–633.

[34] H. Wiedersich, Hardening mechanisms and the theory of deformation, J. Met. 16 (1964) 425–430.

[35] U. F. Kocks, Laws for work-hardening and low-temperature creep, J. Eng. Mater. Tech., ASME 98 (1976) 76–85.

[36] J. Hirth, J. Lothe, Theory of Dislocations, Krieger, 1982.

[37] M. Werner, Temperature and strain-rate dependence of the flow stress of ultrapure tantalum single crystal, Phys. Status Solidi A 104 (1987) 63–78.

[38] H. Lim, J. D. Carroll, C. C. Battaile, T. E. Buchheit, B. L. Boyce, C. R. Weinberger, Grain-scale experimental validation of crystal plasticity finite element simulations of tantalum oligocrystals, Int. J. Plast. 60 (2014) 1–18.

[39] J. L. Chaboche, Continuum damage mechanics: a tool to describe phenomena before crack initiation, Null. Eng. Des. 79 (1981) 309–319.

[40] J. Lemaitre, Coupled elasto-plasticity and damage constitutive equations, Computer Methods in Applied Mechanics and Engineering 51 (1985) 31–49.

[41] D. P. Field, J. M. Yanke, E. V. McGowan, C. A. Michaluk, Microstructurual development in asymmetric processing of tantalum plate, Journal of Electronic Materials 34 (2005) 1521–1525.